Journal of Crystal Growth 89 (1988) 405–414
North-Holland, Amsterdam

MORPHOLOGICAL STABILITY ANALYSIS OF DIRECTIONAL SOLIDIFICATION IN THIN SAMPLES WITH LATERAL HEAT TRANSFER

Jorge VIÑALS

Department of Physics, Carnegie–Mellon University, Pittsburgh, Pennsylvania 15213-3890, USA

R.F. SEKERKA

Departments of Physics and Mathematics, Carnegie–Mellon University, Pittsburgh, Pennsylvania 15213-3890, USA

and

P.P. DEBROY

Department of Physics, Carnegie–Mellon University, Pittsburgh, Pennsylvania 15213-3890, USA

Received 11 November 1987; manuscript received in final form 29 January 1988

Recent experimental evidence indicates that the onset of instability of a planar interface during the directional solidification of a binary system depends on the thickness of the sample. We have investigated the effect that finite lateral heat transfer between a thin sample and the containing cell can have on the morphological stability problem. We have found that such an effect contributes significantly to the stability of the planar interface when $D_T \approx v\sqrt{d/h'}$. D_T is the thermal diffusivity, v the pulling speed and d the thickness of the sample. h' is a heat transfer coefficient in a phenomenological law according to which the heat flux between the sample and the cell is given by the product of h′ with the temperature difference between the sample and the cell. Since it appears that $D_T/v \gg \sqrt{d/h'}$ in the above mentioned experiment, there are probably no appreciable effects arising from a finite lateral heat transfer in the experimentally relevant range of velocities and thicknesses, given a reasonable estimate of the heat transfer coefficient h'. However, h' might be smaller than we have estimated and it would be interesting to determine it experimentally in order to conclusively rule out finite lateral heat transfer alone as the origin for the thickness dependence of the critical velocity observed in the experiments.

1. Introduction

The directional solidification of a binary alloy in involves the uniform motion of the sample relative to its thermal environment [1,2]. Under steady state conditions the solid–liquid interface moves at constant velocity, and, in the case of a single phase solid, there exist simple analytical solutions describing the uniform motion of a planar front. However, it is well known that an instability of the planar interface can occur as a consequence of the buildup of solute ahead of the moving interface [3]. The interface then develops a more complicated cellular structure [4–10] which can also, eventually, reach steady state motion. When the degree of instability increases, dendritic patterns have been observed and even chaotic motion.

The onset of instability of a planar interface has been thoroughly studied theoretically under a wide variety of situations. Linear stability analyses are continually being extended to encompass more complex situations. However, the fact that some of the thermophysical parameters required in the theoretical analyses are not well known in many cases, has often precluded a precise comparison between the experimental measurements and the theoretical calculations (a review of the experimental measurements on the onset of instability can be found in refs. [2,11]). There are, in ad-

0022-0248/88/$03.50

dition, several other effects which are normally ignored in the calculations but that presumably can after the stability of the planar interface (e.g., at high velocities the distribution coefficient must be considered a function of velocity [12]; interfacial kinetic effects at the interface become relevant also so high velocities and the interface deviates from local equilibrium [13], etc.).

A class of effects which have not yet been analyzed in detail are related to the finite lateral thickness of the samples used in some experiments. It has been tacitly assumed that the critical values of the parameters at the onset of instability would be the same as those for infinitely thick samples and, thus, thickness independent. Recent experimental evidence [9], however, clearly indicates that the onset of instability for a planar interface depends on the thickness of the sample. For thin samples, the critical velocity at the onset of instability is seen to increase with thickness. At larger thickness, the critical velocity becomes independent of the thickness (within the precision of the experiment) and at still larger thickness new kinds of instabilities are found in which several layers of cells can be observed.

The fact that the sample has a finite thickness can have several effects on the stability of the solidifying front. On the one hand, the condition of mechanical equilibrium between the solid, melt and container determines the existence of a finite contact angle. Since the Gibbs–Thompson equation at the interface contains its mean curvature, the existence of a meniscus in the direction perpendicular to the motion of the interface introduces into the problem a finite second radius of curvature. This effect has been recently analyzed by Caroli, Caroli and Roulet [14] who have shown that the onset of instability depends explicitly on the thickness of the sample. The second effect, which we wish to investigate in this paper, is related to the existence of a lateral heat transfer between the cell that contains the sample and the sample itself. Unless there is perfect thermal contact between the cell and the sample, the temperature in the sample at a given distance from the interface, z (see fig. 1), will not necessarily be equal to the temperature of the cell (externally imposed) at the same point z. Such a deviation

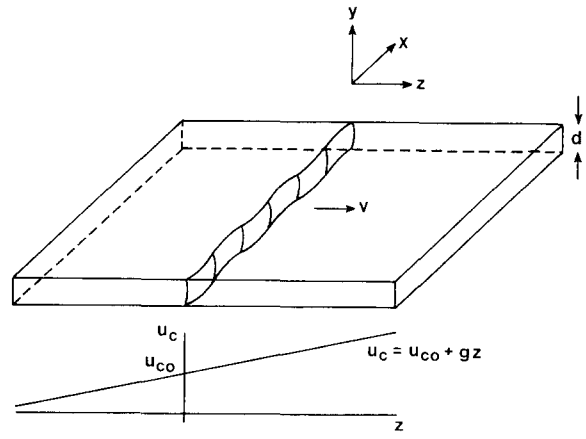

Fig. 1. Schematic representation of a prototypical directional solidification experiment.

may become especially important in the interface region and contribute directly to the stability of the interface.

The analysis of the effect that lateral heat transfer can have on morphological stability during solidification processes was first addressed by Temkin and Polyakov [15]. They considered the solidification of a pure liquid in contact with a thermostat at uniform temperature while allowing for a finite heat transfer between the sample and the thermostat. They found that the heat transfer conditions do affect the stability of the solid–liquid interface. We will consider, instead, a thermal environment in which the temperature is not uniform but, rather, in which there is a constant gradient, as it is appropriate for a directional solidification experiment. Since we are concerned with thin samples, we develop an approximate two-dimensional set of equations by averaging temperature and concentration fields over the direction perpendicular to the direction of motion of the interface (y direction, see fig. 1). We thus will ignore temperature or concentration inhomogeneities along this direction. This set of equations also has a steady-state planar front solution. Its properties will be discussed in section 2. Section 3 is devoted to a linear stability analysis of the steady planar front solution. Unless the phenomenological heat transfer coefficient introduced in our model is smaller than we have estimated, we find that lateral heat transfer does not modify appre-

ciably the onset of instability in the range of parameters which is relevant to the experimental conditions. It would be very interesting, however, to determine the value of the heat transfer coefficient experimentally in order to conclusively rule out finite lateral heat exchange alone as the origin of the thickness dependent critical velocity seen in the experiments.

2. Model equations

We consider the solidification of a binary alloy which is being pulled at constant speed (v) in an environment in which there is a constant temperature gradient (fig. 1). The basic equations that govern the motion of the solid–liquid interface are the heat flow equation in the solid and in the liquid and the diffusion equation in the liquid (we will neglect solute diffusion in the solid). We choose a coordinate system (x', y', z') moving at constant velocity v in the solidification direction which is along the z' axis:

$$D\nabla'^2 c + v\frac{\partial c}{\partial z'} = \frac{\partial c}{\partial t'}, \tag{1a}$$

$$D_s\nabla'^2 T_s + v\frac{\partial T_s}{\partial z'} = \frac{\partial T_s}{\partial t'}, \tag{1b}$$

$$D_\ell\nabla'^2 T_\ell + v\frac{\partial T_\ell}{\partial z'} = \frac{\partial T_\ell}{\partial t'}. \tag{1c}$$

$c(x', y', z', t')$ is the solute concentration in the liquid and $T_s(x', y', z', t')$ and $T_\ell(x', y', z', t')$ denote the temperatures in the solid and liquid respectively. D is the solute diffusion constant and D_s and D_ℓ are the solid and liquid thermal diffusivities respectively. The appropriate boundary conditions at the solid–liquid interface (defined by $z' = \xi(x', y', t')$) are:

$$T_\ell = T_s = T_M + m'c - T_M\Gamma'K', \tag{2a}$$

$$\Delta c\left(v + \frac{\partial \xi'}{\partial t'}\right)\hat{n}\hat{k} = -D(\nabla' c)_I\hat{n}, \tag{2b}$$

$$L_0\left(v + \frac{\partial \xi'}{\partial t'}\right)\left(1 + (c_\ell - c_s)\frac{T_\ell - T_M}{L_0}\right)\hat{n}\hat{k} = \left[-k_\ell(\nabla' T_\ell)_I + k_s(\nabla' T_s)_I\right]\hat{n}, \tag{2c}$$

which are the condition of local thermodynamic equilibrium at the interface, the conservation of solute and the conservation of heat respectively. T_M is the melting temperature of the pure substance, m' is the slope of the liquidus, Γ' is the capillary constant given by $\Gamma' = \sigma/L_0$ (σ is the solid–liquid surface tension and L_0 is the latent heat of fusion per unit volume of crystal at T_M) and K' is the mean curvature of the interface. $\Delta c = (1 - k_p)c_\ell$ is the equilibrium miscibility gap (k_p is the partition coefficient), $\hat{n}$ is the unit normal pointing towards the liquid and $\hat{k}$ is the unit vector in the z' direction. k_ℓ, c_ℓ and k_s, c_s are the thermal conductivities and specific heat per unit volume of the liquid and solid respectively.

We have to supplement these boundary conditions at the solid–liquid interface with boundary conditions at the walls of the container and far-field conditions for the concentration and temperature fields. We take the temperature of the cell which contains the sample to be only a function of z':

$$T_c(z') = T_{c0} + g'z'. \tag{3}$$

In order to account for a finite heat transfer from the sample to the cell, we assume that the heat flux to the plates is simply proportional to the difference between the average temperature of the sample (to be defined below) and the temperature of the cell:

$$-\hat{j}(\nabla' T_s)_{y' = \pm d/2} = \pm h_s'(\bar{T}_s - T_c), \tag{4a}$$

$$-\hat{j}(\nabla' T_\ell)_{y' = \pm d/2} = \pm h_\ell'(\bar{T}_\ell - T_c), \tag{4b}$$

where $\hat{j}$ is the unit vector in the y' direction and h_s' and h_ℓ' are two phenomenological coefficients. Since there is not flux of solute through the walls of the container, we have taken as boundary condition for the concentration field:

$$(\nabla' c)_{y' = \pm d/2} = 0. \tag{5}$$

We will be concerned with thin samples such that the concentration or temperature fields do not vary appreciably in the y' direction (see fig. 1). This fact allows us to reduce the full three-dimensional problem to an approximate effective

problem in two dimensions. We define average quantities through.

$$\bar{A}(x',\, z',\, t') = \frac{1}{d}\int_{-d/2}^{d/2} A(x',\, y',\, z',\, t')\, dy', \tag{6}$$

where A is the concentration or temperature fields and the equation that defines the location of the interface. The diffusion equation for the average concentration field $\bar{c}(x',\, z',\, t')$ is identical to the diffusion equation for $c(x',\, y',\, z',\, t')$. The heat flow equations for $\bar{T}_s(x',\, z',\, t)$ and $\bar{T}_\ell(x',\, z',\, t')$ transform to:

$$D_s \nabla'^2 \bar{T}_s + v\frac{\partial \bar{T}_s}{\partial z'} - \frac{2h_s' D_s}{d}\left(\bar{T}_s - T_c\right) = \frac{\partial \bar{T}_s}{\partial t'}, \tag{7a}$$

$$D_\ell \nabla'^2 \bar{T}_\ell + v\frac{\partial \bar{T}_\ell}{\partial z'} - \frac{2h_\ell' D_\ell}{d}\left(\bar{T}_\ell - T_c\right) = \frac{\partial \bar{T}_\ell}{\partial t'}. \tag{7b}$$

We next introduce dimensionless variables (unprimed) as follows: we rescale lengths by the diffusion length l: $l = D/v$, and time by $\tau = D/v^2$. We define dimensionless fields $\phi = \bar{c}/c_\infty$, where c_∞ is the solute concentration at infinity:

$$u_s = k_\ell\left(\bar{T}_s - T_M\right)/DL_0,$$

$$u_\ell = k_\ell\left(\bar{T}_\ell - T_M\right)/DL_0,$$

$$u_c = k_\ell\left(T_c - T_M\right)/DL_0.$$

We also define

$$\epsilon_s = D/D_s, \quad \epsilon_\ell = D/D_\ell,$$

$$h_\ell = 2l^2 h_\ell'/d, \quad h_s = 2l^2 h_s'/d,$$

$$g = lk_\ell g'/DL_0, \quad \Gamma = \sigma T_M k_\ell / lDL_0^2,$$

$$m = m' c_\infty k_\ell / DL_0.$$

The resulting dimensionless equations are:

$$\nabla^2\phi + \frac{\partial \phi}{\partial z} = \frac{\partial \phi}{\partial t}, \tag{8a}$$

$$\nabla^2 u_s + \epsilon_s \frac{\partial u_s}{\partial z} - h_s(u_s - u_c) = \epsilon \frac{\partial u_s}{\partial t}, \tag{8b}$$

$$\nabla^2 u_\ell + \epsilon_\ell \frac{\partial u_\ell}{\partial z} - h_\ell(u_\ell - u_c) = \epsilon_l \frac{\partial u_\ell}{\partial t}. \tag{8c}$$

Note, however, that the temperature field in the sample has to change, at least, very close to the container walls so as to accommodates the finite heat transfer to the cell. We will assume however that such a change takes place in a very small region around the walls of thickness δ, small compared to the thickness of the sample d ($\delta/d \ll 1$). Provided that $\delta/d \ll 1$, the boundary conditions (2) have the same form when written in terms of the corresponding averaged quantities:

$$u_s = u_\ell = m\phi - \Gamma K, \tag{9a}$$

$$\left(1 + \frac{\partial \xi}{\partial t}\right)(1 + \alpha u_\ell)\hat{n}\hat{k} = \left[-(\nabla u_\ell)_1 + q_p(\nabla u_s)_1\right]\hat{n}, \tag{9b}$$

$$\left(1 + \frac{\partial \xi}{\partial t}\right)(1 - k_p)\phi\hat{n}\hat{k} = -\nabla\phi\hat{n}, \tag{9c}$$

with $q_p = k_s/k_\ell$. We have defined $\alpha = (1 - q_p D_\ell/D_s)\epsilon_\ell$. The dimensionless temperature of the plates is given by $u_c(z) = u_{c0} + gz$.

2.1. Steady state solution

The previous set of equations and boundary conditions admits a steady state solution in which a planar interface, located at $z = 0$, moves at constant velocity in the laboratory frame. We choose the following far field conditions: the solute concentration at infinity is $\phi_\infty = 1$ and the temperature gradient in the solid and in the liquid approach the temperature gradient of the cell far away from the solid–liquid interface. Other choices for the far field conditions on the temperature fields (e.g. fixed the temperature of the sample to be equal to the temperature of the container at a given distance ahead and behind the interface) lead to the same results concerning the stability of the planar interface. The solution for the dimensionless concentration is:

$$\phi^{(0)}(z) = 1 + \frac{1 - k_p}{k_p} e^{-z}. \tag{10}$$

The steady state solutions for the temperature fields are:

$$u_\ell^{(0)}(z) = u_{c0} + \frac{\epsilon_\ell g}{h_\ell} + gz + B_\ell \exp(\lambda_2^\ell z), \quad (11a)$$

$$u_s^{(0)}(z) = u_{c0} + \frac{\epsilon_s g}{h_s} + gz + A_s \exp(\lambda_1^s z), \quad (11b)$$

with

$$\lambda_2^\ell = -\tfrac{1}{2}\epsilon_\ell - \sqrt{\tfrac{1}{4}\epsilon_\ell^2 + h_\ell}, \quad (12a)$$

$$\lambda_1^s = -\tfrac{1}{2}\epsilon_s + \sqrt{\tfrac{1}{4}\epsilon_s^2 + h_s}. \quad (12b)$$

The Gibbs–Thompson equation yields:

$$B_\ell = \frac{m}{k_p} - \left(u_{c0} + \frac{\epsilon_\ell g}{h_\ell}\right), \quad (13)$$

and from the continuity of temperature, we obtain:

$$A_s = B_\ell - g\left(\frac{\epsilon_s}{h_s} - \frac{\epsilon_\ell}{h_\ell}\right). \quad (14)$$

Finally, the heat balance equation allows us to determine u_{c0}:

$$u_{c0} = \left[1 + \frac{m}{k_p}\alpha + (1-q_p)g + \left(\frac{m}{k_p} - \frac{\epsilon_\ell g}{h_\ell}\right)\lambda_2^\ell - q_p\left(\frac{m}{k_p} - \frac{\epsilon_s g}{h_s}\right)\lambda_1^s\right]\left(\lambda_2^\ell - q_p\lambda_1^s\right)^{-1}, \quad (15)$$

and the steady state solution is completely determined.

The temperature gradients at the liquid and solid side of the interface are:

$$G_\ell^{(0)} \equiv \left.\frac{du_\ell^{(0)}}{dz}\right|_{z=0} = g + B_\ell\lambda_2^\ell, \quad (16a)$$

$$G_s^{(0)} = \left.\frac{du_s^{(0)}}{dz}\right|_{z=0} = g + A_s\lambda_1^s. \quad (16b)$$

Before proceeding with the stability analysis, it is useful to analyze in somewhat more detail the properties of the steady solutions which we have obtained. In what follows, we will only consider the case $h_s = h_\ell \equiv h$ for simplicity. We also use the thermophysical parameters for the organic compound CBr_4 used in the experiments by de Cheveigné et al. [9] (table 1). For very small thicknesses, $h \gg \epsilon^2$ and $G_\ell^{(0)}$ becomes independent of d,

$$G_\ell^{(0)} \approx g - \frac{1 + \alpha m/k_p - g(q_p - 1)}{1 + q_p}.$$

Also, when the thickness is large (such that $h \ll \epsilon^2$),

$$G_\ell^{(0)} \approx -1 - \alpha m/k_p + q_p g,$$

again independent of the thickness. The crossover region is determined by $\epsilon^2 \sim h$, or, equivalently, $D_\ell \sim \sqrt{d/h'}\,v$. In the experiments described in ref. [9], which involved CBr_4 (the appropriate thermophysical parameters are listed in table 1), $\epsilon_\ell \approx \epsilon_s \approx 0.02$. On the other hand

$$h = \frac{2l^2h'}{d} = \frac{2D^2h'}{dv^2}.$$

It would seem reasonable that h', as defined in eq.

Table 1
Thermophysical parameters of CBr_4 from ref. [9]; also listed is some additional information on the experiments, which is relevant to the calculation

Thermophysical parameters	
Slope of the liquidus (m)	−2.9 K/mol%
Partition coefficient (k_p)	0.16
Melting temperature of the pure substance (T_M)	366.45 K
Latent heat of fusion (L_0)	2.41 cal/g
Surface tension (σ)	1.675×10^{-7} cal/cm^2
Density of the solid (ρ_s)	3.4 g/cm^3
Density of the liquid (ρ_ℓ)	2.96 g/cm^3 [a]
Diffusion constant (D)	1.2×10^{-5} cm^2/s
Specific heat of the solid (c_s)	0.13 cal/g·K
Specific heat of the liquid (c_ℓ)	0.11 cal/g·K
Thermal conductivity of the solid (k_s)	2×10^{-4} cal/s·cm·K [a]
Thermal conductivity of the liquid (k_ℓ)	2×10^{-4} cal/s·cm·K [a]
Experimental conditions	
Concentration at infinity (c_∞)	0.12 mol%
Imposed thermal gradient (g')	70–120 K/cm
Sample thickness (d)	5–150 μm
Pulling speed (v)	1–10 μm/s

[a] Values shown are estimates.

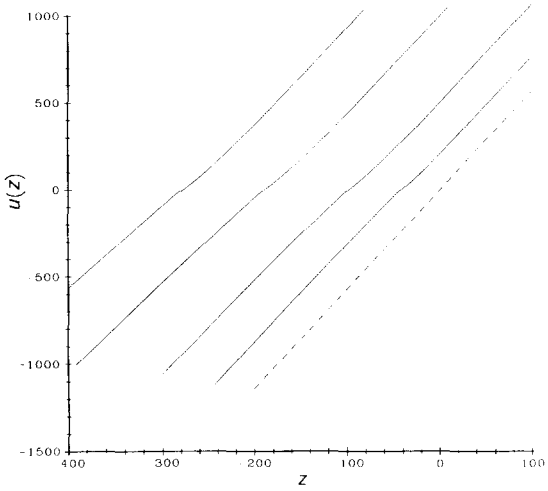

Fig. 2. Dimensionless temperature fields in the liquid and solid phases as a function of the dimensionless position. The pulling speed is $v = 3$ μm/s. The solid lines represent the temperature fields for different lateral thicknesses of the sample. The thicknesses shown are from right to left: $d = 1$, 3, 5 and 10 μm. The dashed line is the dimensionless temperature of the container.

(4), is bounded by $1/d$, i.e. $h' \geq 1/d$. Taking $h' = 1/d$ and typical values for the thickness and pulling speed: $v = 10$ μm/s and $d = 10$ μm, we obtain $h' \sim 100$. Thus, $h \gg \epsilon^2$ and the gradient in the liquid becomes independent of the thickness. As it will discussed below, the parameter that controls the stability of the planar interface is proportional to $1 + 2G_\ell^{(0)}$. As a consequence, unless h' is smaller than we have estimated, we would not expect any appreciable effect from lateral heat transfer on the stability of the planar interface in the experimentally relevant range of velocities and ticknesses.

The properties of the steady state solution are also seen to depend very sensitively on the ratio of thermal conductivities q_p. We consider first the case in which the thermal conductivities of the solid and the liquid are equal. Fig. 2 shows the temperature field as a function of position for different thicknesses d. For the sake of clarity, we have chosen as origin of coordinates in this figure the point at which the dimensionless temperature of the cell, u_c, is zero. Consequently, the steady state planar interface would be located at $z_0 = -u_{c0}/g$ in fig. 1. The steady state solution for the concentration field is

$$\phi^{(0)} = 1 + \left(\frac{1 - k_p}{k_p}\right) e^{-(z - z_0)}.$$

The steady state solution for the temperature fields can similarly be obtained by replacing z by $z - z_0$ in eq. (11). We note that the temperature of the interface remains constant for all thicknesses ($u_s = u_\ell = m/k_p$), but its location moves in the negative z-direction (towards cooler regions as given by the temperature of the cell) when the thickness increases. Fig. 3 presents the gradient in the liquid side of the interface $G_\ell^{(0)}$ also as a function of the thickness. We have used in our calculations (shown in figs. 2–9) what appears to be an unrealistic value of $h' = 2 \times 10^{-5}$ cm^{-1}, such that the effects introduced by lateral heat transfer are seen in the experimentally relevant range of velocities and thickness. The same behavior would be observed for higher values of h', although shifted to larger values of the thickness.

We have also considered the case in which the thermal conductivity of the solid is larger than the thermal conductivity of the liquid. We show in fig. 4 the temperature in the solid and the liquid for different thicknesses. The temperature profiles are concave in this case, whereas they were convex in

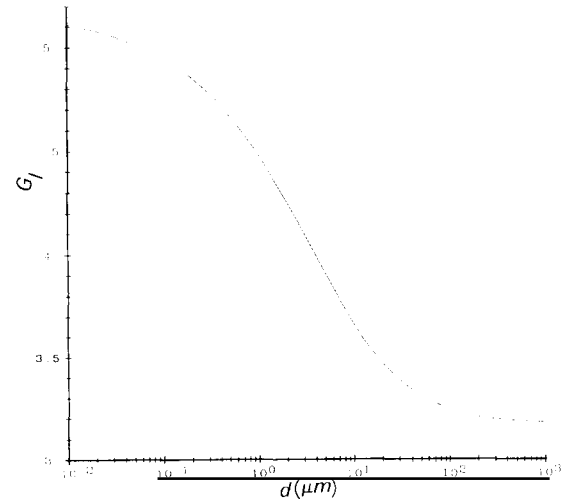

Fig. 3. Dimensionless temperature gradient in the liquid side of the interface as a function of the thickness of the sample. The pulling speed is $v = 3$ μm/s. The thermal conductivities of the solid and liquid are equal ($q_p = 1$).

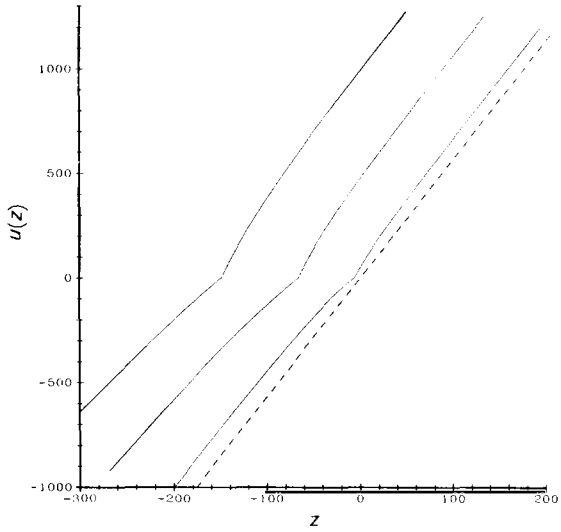

Fig. 4. Dimensionless temperature in the liquid and solid phases as a function of the dimensionless position. The pulling speed is $v = 3$ μm/s. The thermal conductivity of the solid is larger than the thermal conductivity of the liquid ($q_p = 2.7$). The solid lines represent the temperature fields for different lateral thicknesses of the sample. The thicknesses shown are from right to left: $d = 1$, 2 and 3 μm. The dashed line is the dimensionless temperature of the container.

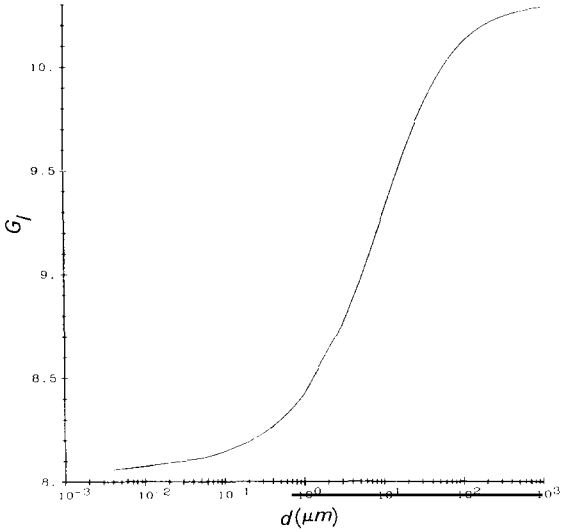

Fig. 5. Dimensionless temperature gradient in the liquid side of the interface as a function of the thickness of the sample. The pulling speed is $v = 3$ μm/s. The thermal conductivity ratio is $q_p = 2.7$.

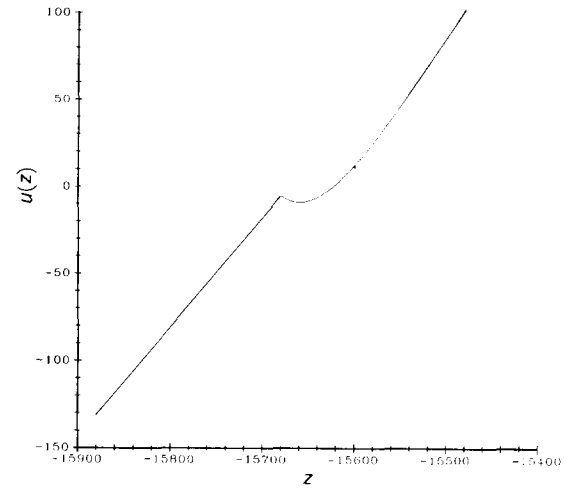

Fig. 6. Dimensionless temperature in the liquid and solid phases as a function of the dimensionless position. $q_p = 2.7$ and the pulling speed is $v = 20$ μm/s. The thickness of the sample is d = 20 μm.

the case presented in the previous section. The interface location also moves towards colder regions as the thickness of the sample increases. The gradient in the liquid $G_\ell^{(0)}$ is shown in fig. 5. We note, however, that for high enough velocities (where the latent heat contribution becomes important), the temperature profiles are similar to the case of equal conductivities (fig. 6), even though $q_p \neq 1$.

3. Stability analysis

We perturb the interface, temperature and concentration fields about their steady state value, and all the equations and boundary conditions are linearized with respect to the amplitude of these perturbations. The perturbation analysis is performed in the quasistationary approximation [1,16]. The perturbations for the fields and the interface considered are as follows:

$$\phi(x, z, t) = \phi^{(0)}(z) + \epsilon\hat{\phi}\, e^{-qz}\, e^{ikx+\omega t}, \quad (17a)$$

$$u_\ell(x, z, t) = u_\ell^{(0)}(z) + \epsilon\hat{u}_\ell\, e^{-q_\ell z}\, e^{ikx+\omega t}, \quad (17b)$$

$$u_s(x, z, t) = u_s^{(0)}(z) + \epsilon\hat{u}_s\, e^{q_s z}\, e^{ikx+\omega t}, \quad (17c)$$

$$z = \epsilon\xi(x, t) = \epsilon\xi_0\, e^{ikx+\omega t}. \quad (17d)$$

where ϵ is a small parameter, $\hat{\phi}$, $\hat{u}_\ell$, $\hat{u}_s$ and ξ_0 are constants and k is the wavevector of a sinusoidal

perturbation. Linearization in ϵ of the equations and boundary conditions leads to the following system of algebraic equations for the amplitudes of the perturbations:

$$\xi_0\left(1-k_p+\frac{1-k_p}{k_p}\omega\right)-\hat{\phi}(q+k_p-1)=0, \tag{18a}$$

$$\xi_0\left[\alpha G_\ell^{(0)}+\omega+\alpha\omega\frac{m}{k_p}+B_\ell(\lambda_2')^2-q_pA_s(\lambda_1^s)^2\right] +\hat{u}_\ell(\alpha-q_\ell)-\hat{u}_sq_pq_s=0, \tag{18b}$$

$$\xi_0(G_\ell^{(0)}-G_s^{(0)})+\hat{u}_\ell-\hat{u}_s=0, \tag{18c}$$

$$\xi_0\left(G_\ell^{(0)}+\Gamma k^2-\frac{m(k_p-1)}{k_p}\right)+\hat{u}_\ell-m\hat{\phi}=0, \tag{18d}$$

with

$$q=\tfrac{1}{2}+\sqrt{\tfrac{1}{4}+k^2}, \tag{19a}$$

$$q_\ell=\tfrac{1}{2}\epsilon_\ell+\sqrt{\tfrac{1}{4}\epsilon_\ell^2+k^2+h}, \tag{19b}$$

$$q_s=-\tfrac{1}{2}\epsilon_s+\sqrt{\tfrac{1}{4}\epsilon_s^2+k^2+h}. \tag{19c}$$

The compatibility of this system of homogeneous linear equations requires that the determinant of the coefficients vanish. This yields an equation for ω as a function of the wavevector k and the other independent parameters:

$$\omega=\frac{\bar{k}\left(\dfrac{q-1}{q-1+k_p}-\dfrac{A}{k_p}k^2-G\right)+H}{\dfrac{\bar{k}}{q-1+k_p}+\dfrac{1}{I}}, \tag{20}$$

where we have defined:

$$\bar{k}=q_\ell+q_pq_s-\alpha, \tag{21a}$$

$$A=\Gamma k_p^2/m(k_p-1), \tag{21b}$$

$$G=\frac{k_p}{m(k_p-1)}\frac{1}{\bar{k}}\left[q_pq_sG_s^{(0)}+q_\ell G_\ell^{(0)}\right], \tag{21c}$$

$$I=\frac{m(k_p-1)}{k_p(1+\alpha m/k_p)}, \tag{21d}$$

$$H=\frac{k_p}{m(k_p-1)}\left[A_s(\lambda_1^s)^2q_p-B_\ell(\lambda_2')^2\right]. \tag{21e}$$

A is the absolute stability parameter introduced by Mullins and Sekerka [2], I can be regarded as a dimensionless concentration at infinity and G is related to the conductivity weighted average of the thermal gradients at the interface. The effect of the heat losses is contained in $\bar{k}$, G and H; although, as we will argue below, G is the dominant parameter.

Although the actual calculations which will be shown below have been performed with the exact relation (20), it is useful to simplify it by considering reasonable approximations. Given the values of the thermophysical parameters shown in table 1, we have $\epsilon_\ell\approx\epsilon_s\approx 0.02$ whereas the dimensionless critical wavevector is of order 1. As a consequence,

$$\bar{k}\approx(1+q_p)\sqrt{k^2+h},$$

so $\bar{k}$ is approximately proportional to the wavevector k except for very small thicknesses or very small velocities where it is simply a constant. Secondly, as mentioned above, the capillarity related absolute stability parameter A is not affected by the thickness of the sample. Also, given that $\epsilon_\ell^2\approx\epsilon_s^2\ll k^2$, $q_\ell\approx q_s\approx\sqrt{k^2+h}$. Then, recalling that eq. (9) for the conservation of heat at a planar interface can be rewritten as: $1+\alpha m/k_p=G_\ell^{(0)}+q_pG_s^{(0)}$, we obtain (we also neglect $\alpha=-3.55\times10^{-3}$, given in table 1):

$$G\approx\frac{k_p}{m(k_p-1)(1+q_p)}(1+2G_\ell^{(0)}). \tag{22}$$

This parameter G is the same as that defined in eq. (15) in ref. [2], where lateral heat losses were not included [17]. Finally, the parameter H in (20) is a constant independent of wavevector and small in magnitude. Thus, the analysis in ref. [2] essentially applies to our present case except for an important modification. Whereas it is customary to treat the gradient in the liquid $G_\ell^{(0)}$ as an independent variable, here it seems more natural to hold the gradient in the glass, g, constant instead [18].

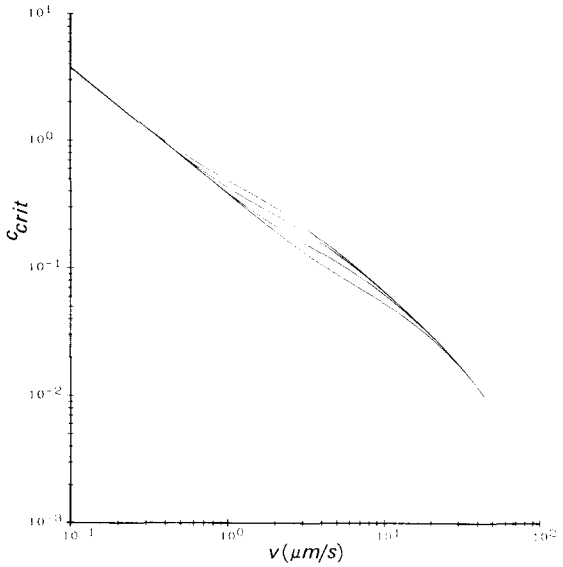

Fig. 7. Critical concentration (in wt%) as a function of the pulling speed (in μm/s). $q_p = 2.7$. The thicknesses shown are: $d = 1$, 5, 20 and 50 μm.

If we further consider the limit $\epsilon^2 \ll h$, we obtain that:

$$z_0 = \frac{m}{k_p} - \frac{1 + g(1 - q_p)}{\sqrt{h}\,(1 + q_p)}; \tag{23}$$

z_0 is the location of the steady state interface if we choose as origin of coordinates the point at which the dimensionless temperature of the cell, u_c, is zero. On the other hand, the gradient in the liquid simply becomes:

$$G_\ell^{(0)} = g - \frac{1 + (1 - q_p)g}{1 - q_p \lambda_1^s / \lambda_2^\ell}, \tag{24}$$

and the parameter G becomes independent of the thickness since both λ_1^s and λ_2^ℓ are proportional to $\sqrt{h}$ (eq. (12)).

We finally present the results of the linear stability calculation, with the choice of the heat transfer coefficient discussed above. Fig. 7 shows the concentration at the onset of instability as a function of the front velocity for $q_p = 2.7$ and different thicknesses. There is a range of velocities in which the onset of instability of the planar interface appreciably depends on the thickness,

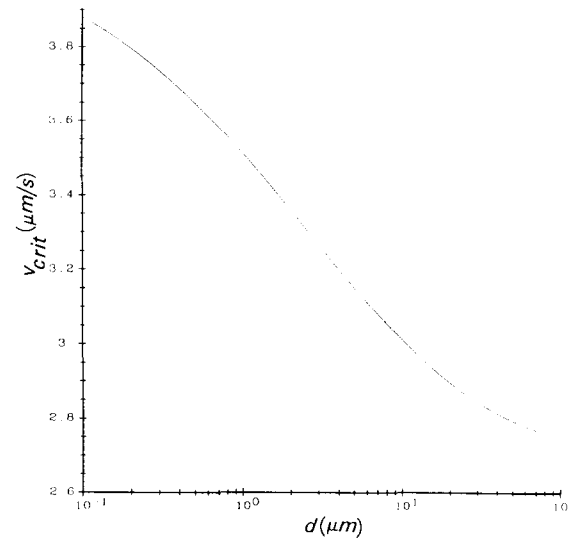

Fig. 8. Critical velocity versus thickness of the sample for $q_p = 1$.

precisely when $\epsilon^2 \sim h$. Finally, figs. 8 and 9 show the critical velocity as a function of the thickness of the sample. Note how the behavior of the critical velocity is identical to the behavior of $G_\ell^{(0)}$ shown in figs. 3 and 5. Both, for very small and very large thicknesses, the critical velocity becomes independent of the thickness of the sample. As it has been discusses above, only for thick-

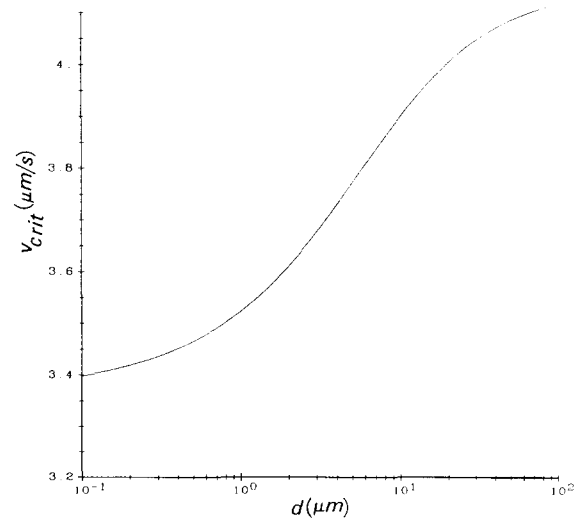

Fig. 9. Critical velocity versus thickness of the sample for $q_p = 2.7$.

nesses such that $\epsilon^2 \sim l^2 h'/d$ the finite heat transfer to the cell significantly modifies the onset of instability. It would appear that the experiments described in ref. [9] are in the range of velocities and thicknesses such that $\epsilon^2 \ll l^2 h'/d$, given our estimate of the heat transfer coefficient and, thus, in the range in which the effects of lateral heat transfer become negligible. We point out, however, that to completely elucidate the relevance of lateral heat transfer in those experiments, it would be desirable to have a more precise determination of the phenomenological heat transfer coefficient.

Acknowledgements

This work has been supported by NSF Grant No. DMR-8409397.

References

[1] J.S. Langer, Rev. Mod. Phys. 52 (1980) 1.
[2] S.R. Coriell, G.B. McFadden and R.F. Sekerka, Ann. Rev. Mater. Sci. 15 (1985) 119.
[3] W.W. Mullins and R.F. Sekerka, J. Appl. Phys. 35 (1964) 444.
[4] G. Dee and R. Mathur, Phys. Rev. B27 (1983) 7073.
[5] G.B. McFadden and S.R. Coriell, Physica 12D (1984) 253.
[6] L.H. Ungar and R.A. Brown, Phys. Rev. B29 (1984) 1367; L.H. Ungar, M.J. Bennett and R.A. Brown, Phys. Rev. B31 (1985) 5923; L.H. Ungar and R.A. Brown, Phys. Rev. B31 (1985) 5931.
[7] A. Karma, Phys. Rev. Letters 57 (1986) 585; Phys. Rev. A34 (1986) 4353.
[8] K. Somboonsuk, J.T. Mason and R. Trivedi, Met. Trans. A15 (1984) 967.
[9] S. de Cheveigné, C. Guthmann and M.M. Lebrun, J. Physique 47 (1986) 2095.
[10] J. Bechhoefer and A. Libchaber, Phys. Rev. A35 (1986) 1393.
[11] R.F. Sekerka, in: Crystal Growth: An Introduction, Ed. P. Hartman (North-Holland, Amsterdam 1973) pp. 403–443; R.T. Delves, in: Crystal Growth, Ed. B.R. Pamplin (Pergamon, Oxford, 1974) pp. 40–103; M.C. Flemings, Solidification Processing (McGraw-Hill, New York, 1974).
[12] R.F. Wood, Appl. Phys. Letters 37 (1980) 302; M.J. Aziz, J. Appl. Phys. 53 (1982) 1158; K.A. Jackson, G.H. Gilmer and H.J. Leamy, in: Laser and Electron Beam Processing of Materials, Eds. C.W. White and P.S. Pearcy (Academic Press, New York, 1980); F.X. Kelly and L.H. Ungar, Phys. Rev. B34 (1986) 1746.
[13] See, for example: J.S. Langer, in: Chance and Matter, Les Houches Summer School, July 1986.
[14] B. Caroli, C. Caroli and B. Roulet, J. Crystal Growth 76 (1986) 31.
[15] D.E. Temkin and V.B. Polyakov, Soviet Phys.-Cryst. 21 (1977) 374.
[16] R.F. Sekerka, in: Crystal Growth, Ed. H.S. Peiser (Pergamon, Oxford, 1967) p. 691.
[17] The linear stability analysis presented in ref. [2] involves a time dependent perturbation as opposed to the time independent one considered here. As a consequence, the dispersion relations obtained are different. The parameter G, however, is the same in both cases.
[18] We note that taking g as control instead of $G_\ell^{(0)}$ results in that for high enough velocities, G can be negative and the system becomes unstable against long wavelength fluctuations.